

ORIGINAL RESEARCH

Methylene Blue Reduces Retinal Cell Inflammation, Apoptosis, and Oxidative Stress in a Rat Model of Diabetic Retinopathy via Sirtuin 1 Activation

Huade Mai, Mmed; Chenghong Liu, Mmed; Biwei Fu, Mmed; Xinbo Ji, Mmed; Minghui Chen, Mmed; Yunbo Zhang, Mmed; Yunyun Lin, Mmed; Juming Chen, Mmed; Yanling Song, Mmed; Shenhong Gu, MD

ABSTRACT

Objective • Diabetic retinopathy (DR), characterized by neuronal damage in the retina, is primarily driven by oxidative stress resulting from diabetes (DM). This study investigated the potential effects of methylene blue (MB) on streptozotocin (STZ)-induced DR.

Methods • A rat model of DR was established via STZ injection, while a cell model was created using high-glucose (HG) exposure of human retinal microvascular endothelial cells. Evaluation of oxidative stress markers, pro-inflammatory cytokines, and pro-apoptotic proteins was performed based on their expression profiles in human retinal microvascular endothelial cells.

Results • MB treatment significantly upregulated the expression of sirtuin 1 (SIRT1), which was found to be

downregulated in the retinal tissues of STZ-treated rats and HG-exposed human retinal microvascular endothelial cells, as determined by polymerase chain reaction (PCR). Furthermore, MB therapy effectively suppressed STZ-induced oxidative stress, inflammation, and cell death. Consistent with the *in vivo* findings, MB activated the expression of SIRT1, thereby protecting HG-treated human retinal microvascular endothelial cells against oxidative stress, inflammation, and apoptosis.

Conclusion • These results support the conclusion that MB mitigates DR by activating SIRT1, leading to a reduction of inflammation, apoptosis, and oxidative stress. (*Altern Ther Health Med.* 2023;29(8):156-165).

Huade Mai, Mmed; Xinbo Ji, Mmed; Minghui Chen, Mmed; Yunbo Zhang, Mmed; Yunyun Lin, Mmed; Juming Chen, Mmed; Yanling Song, Mmed; Shenhong Gu, MD; Department of General Practice, First Affiliated Hospital of Hainan Medical University, Haikou, Hainan Province, China. Chenghong Liu, Mmed; Biwei Fu, Mmed; Hainan Medical University, Haikou, Hainan Province, China.

Corresponding author: Shenhong Gu, MD
E-mail: mhd18976088265@163.com

INTRODUCTION

Diabetic retinopathy (DR), a severe microvascular complication associated with diabetes mellitus (DM), is globally recognized as the primary cause of visual impairment and blindness.¹ Current data reveal that DR accounts for approximately 2.4 million incidences of worldwide blindness,² with an annual prevalence rate ranging from 2.2% to 12.7%.³ DR, a disorder characterized by visual impairment, initially manifests as retinal neuronal and vascular dysfunction, which frequently escalates to significant visual acuity loss due to neovascularization.⁴ The methylene blue (MB) pathogenesis of DR has been linked to angiogenesis, oxidative stress, and

chronic inflammation.⁵ Several risk factors such as hyperglycemia, hypertension, advanced age, insulin treatment, elevated fasting blood glucose levels, prolonged DM duration, increased hemoglobin A1c concentration, and dietary habits have all been validated as contributors to the onset and progression of DR.⁶

Despite advancements in amending retinal vascular modifications, DR remains a significant challenge in clinical treatment.⁷ Consequently, there is an urgent need for in-depth molecular studies to devise more effective therapeutic strategies against DR.

Effective glycemic management plays a crucial role in delaying the onset and progression of DR.⁸ Currently, advanced intravitreal treatments employing anti-angiogenic or anti-inflammatory drugs are the most commonly used strategies for treating established DR.⁹ The introduction of these agents has significantly improved the management of vision loss and visual acuity impairment.¹⁰ Nonetheless, the limited availability of approved medications has spurred numerous investigations to search for novel pharmacological approaches. Multiple lines of evidence support the notion that hyperglycemia contributes to the development of DR.¹¹ Excessive formation of reactive oxygen species (ROS) represents the primary mechanism underlying hyperglycemia-induced tissue damage, affecting

retinal arteries, neurons, and glial cells.¹² Consequently, numerous macromolecules are impaired, resulting in oxidative stress markers, such as 8-iso-prostaglandin F2 (iPF2), a well-established indicator of lipid peroxidation.¹³ In addition, oxidative stress alters the activity of antioxidant enzymes, including superoxide dismutase (SOD), which has been shown to be reduced in DM.¹⁴

MB, which belongs to the significant family of phytochemicals, has exhibited a wide range of therapeutic benefits across various clinical conditions, including neurodegeneration and neurological illnesses.^{5,15} MB is renowned for its diverse biological actions, encompassing antioxidant, anti-inflammatory, neuroprotective, hepatoprotective, cardioprotective, and anticancer properties.¹⁶⁻¹⁹ In animal models of retinal neovascularization, MB has demonstrated robust anti-angiogenic properties and has been shown to ameliorate endothelial dysfunction in diabetes.²⁰ Of note, MB's neuroprotective effects have been observed in numerous neurodegenerative disorders.²¹ Our research groups have recently conducted investigations focusing on various MB ester and amide analogues with different alkyl chain lengths, revealing potent neuroprotection *in vitro* via the regulation of neuronal signaling pathways. Among these chemicals, the hexyl and dodecyl amide derivatives of MB exhibited remarkable efficacy and were selected for further study, taking into consideration the improved pharmacokinetic profile typically associated with amide derivatives, including enhanced lipophilicity and resistance to esterase activity.²²

Moreover, compelling evidence suggests that the ability of MB to activate sirtuin 1 (SIRT1) promotes mitochondrial biogenesis and oxygen consumption and activates AMP-activated protein kinase (AMPK), contributing to anti-lipogenesis in the liver.²³ Specifically, a recent study underscored the role of microRNA-377 in DR. The downregulation of this microRNA mitigated high glucose (HG) and hypoxia-induced angiogenic effects, and diminished the release of pro-inflammatory cytokines via the enhancement of SIRT1 activation, thereby attenuating DR.²⁴ Furthermore, prior research exhibited the therapeutic efficacy of the isoflavone formononetin when combined with the induction of SIRT1 expression in the kidney tissues of rats with diabetes,²⁵ significantly alleviating oxidative stress.

Given these findings, we postulated that a potential regulatory interplay exists between MB, SIRT1 and DR. To substantiate this hypothesis, we examined the impact of MB on oxidative stress, the inflammatory response and cell apoptosis within the context of DR, with a specific focus on the activation of SIRT1.

In light of the preceding observations, we posited the existence of a possible regulatory association involving MB, SIRT1, and DR. To scrutinize this hypothesis, we embarked on an exploration of the impact of MB on oxidative stress, the inflammation response, and cellular apoptosis within the framework of DR, specifically considering the activation of SIRT1.

MATERIALS AND METHODS

Ethics Statement

This study received approval from the Medical Ethics Committee of the First Affiliated Hospital of Hainan Medical University (Approval number: HY2022-5545AL) and was conducted in full compliance with the Animal Use Guidelines set forth by the Association for Research in Vision and Ophthalmology (ARVO). All procedures implemented in this study were designed to minimize the number of animals used and their suffering. Comprehensive monitoring was carried out throughout the study, encompassing the animals' health status, dietary intake, and behavior. Prompt attention was given to address any potential discomfort or pain, and necessary measures were taken to ensure the welfare of the animals.

Streptozotocin-induced Rat DR Model Establishment

A total of 80 male Sprague-Dawley (SD) rats weighing 250 to 300 g and meeting specific pathogen-free (SPF) standards, were obtained from Hunan SJA Laboratory Animal Co., Ltd. in Changsha, China. Of these rats, 15 were sham-operated and fed a regular diet, while the remaining 60 rats were fed a high-fat diet. Following a 12-hour fasting period, the rats on the high-fat diet received an intraperitoneal injection of streptozotocin (STZ) dissolved in 0.1 mol/L citrate buffer (pH = 4.5) at a dose of 60 mg/kg. After 72 hours, blood samples were collected from the tail vein to measure blood glucose levels. The sham-operated rats received an injection of an equivalent amount of citric acid buffer, and their blood glucose levels were measured using the Glucotrend-2 offline blood glucose monitoring system (Roche Diagnostics GmbH, Mannheim, Germany). A blood glucose level consistently exceeding 16.7 mmol/L for 1 week indicated successful establishment of the DR model.²⁶ The STZ-treated rats were then given an intraperitoneal injection of either an equal volume of dimethyl sulfoxide (DMSO) or MB. To prepare MB, DMSO was diluted with 100% DMSO. Starting from the day of STZ-induced model establishment, the rats were subcutaneously injected with DMSO (n = 15), 10 mg/kg MB (n = 15), 50 mg/kg MB (n = 15) or 100 mg/kg MB (n = 15) for a duration of 8 weeks. Rats in the sham and STZ groups received equal volumes of normal saline.

Cell Culture and Treatment

Human retinal microvascular endothelial cells (hRMECs) were obtained from the Beijing Beichuang Institute of Biotechnology in Beijing, China. The cells were cultured in Dulbecco's modified Eagle's medium (DMEM; Gibco, Carlsbad, California USA) supplemented with 10% fetal bovine serum (FBS) (Gibco), 100 U/mL penicillin and 100 µg/mL streptomycin. The cell culture was maintained in a 37°C incubator with 5% CO₂. To establish DR cell models, hRMECs were cultured in 70 nM conditions, mimicking the hyperglycemia and hyperlipidemia characteristic of DM. Briefly, the cells were seeded in a 6-cm dish at a density of 2 × 10⁵ cells and incubated at 37°C with 5% CO₂ until reaching

70% to 80% confluence. The day before transfection, the cells were trypsinized, resuspended in the culture medium to obtain a single-cell suspension and then seeded in a 6-well plate at a density of 2×10^5 cells per well. For transfection, 10 μ L of short hairpin RNA against SIRT1 (sh-SIRT1) was mixed with Opti-minimum essential medium (MEM) to a total volume of 250 μ L. After incubating for 5 minutes at room temperature, the samples were mixed with an equal volume of liposome and incubated for 20 minutes to form an shRNA-liposome complex. Subsequently, the complex was added to each well of the 6-well plate at a density of 0.5 nL per well and gently mixed. Following that, 1.5 mL of serum-free DMEM was added to each well, and the cells were cultured at 37°C with 5% CO₂ for 6 hours. Afterward, the medium was replaced with DMEM containing normal serum and the cells were maintained in a 37°C incubator with 5% CO₂.

Cell Counting Kit-8 (CCK-8) Assay

The viability of hRMECs was evaluated following SIRT1 knockdown using the CCK-8 kit (Dojindo Molecular Technologies, Gaithersburg, Maryland USA). The hRMECs were cultured in 96-well plates and transfected with shRNA plasmids for 48 hours. Subsequently, the cells were incubated with 10 μ L of CCK-8 solution for 1 hour in a 37°C incubator with 5% CO₂ and 95% relative humidity. The absorbance value at a wavelength of 450 nm was measured using a microplate reader (Bio-Rad, Hercules, California USA).

Quantification of Levels of Reactive Oxygen Species (ROS), 3,4-Methylenedioxyamphetamine (MDA) and Superoxide Dismutase (SOD)

ROS production in cells was assessed utilizing the CM-H2DCFDA kit (#C6827, Thermo Fisher Scientific, Rockford, Illinois USA). MDA levels and SOD activity were measured using the lipid peroxidation MDA assay kit (#S0131) and WST-8 (CCK-8) SOD assay kit (#S010), respectively, meticulously following the provided instructions. The resulting values were expressed as a percentage of the average absorbance normalized to that of the normal control absorbance.

Nitrite Test

To assess nitric oxide (NO) production, the nitrite content in the supernatant was measured using an oxidized nitrite kit (Beyotime Institute of Biotechnology, Jiangsu, China). Due to the instability of NO, it readily forms nitrates and nitrites in cells. The measurement was performed by following the provided instructions. The supernatant was mixed sequentially with equal volumes of Gris reagent I and Gris reagent II, as instructed. The concentration of nitrites was then determined based on the optical density (OD) value measured at a wavelength of 540 nm using the SmartSpec[™] plus spectrophotometer (Bio-Rad Laboratories, Hercules, California USA).

Enzyme-Linked Immunosorbent Assay (ELISA)

The levels of interleukin-6 (IL-6), tumor necrosis factor α (TNF- α) and C-reactive protein (CRP) in the cell

supernatant were measured using ELISA kits (R & D Systems, Minneapolis, Minnesota USA). The measurements were made following the provided instructions. The SmartSpec Plus spectrophotometer (Bio-Rad Laboratories) was used to obtain the readings.

Hematoxylin-eosin (H&E) Staining

Following ophthalmectomy, the rat eyeballs were immersed in 4% paraformaldehyde for 48 hours to facilitate fixation. The retina and sclera were subsequently dehydrated using a gradient of ethanol and embedded in paraffin. Dewaxing of the paraffin-embedded sections was performed using xylene, followed by successive rinsing with ethanol in decreasing concentrations (99.9%, 97%, 75% and 50%) and distilled water. Subsequently, the sections were subjected to staining with hematoxylin for a duration of 1 to 3 minutes. After each step, the sections were rinsed under running water for 1 minute. Differentiation was achieved by treating the sections with 1% hydrochloric acid alcohol for 20 seconds, followed by rinsing in phosphate-buffered saline (PBS) for 30 seconds. The sections were then stained with eosin for 1 minute, dehydrated using a gradient of ethanol, cleaned with xylene, and ultimately sealed with Histomount mounting solution (Thermo Fisher Scientific). The retinas from each group of rats were observed and photographed using a high-power optical microscope (Olympus Optical Co., Ltd, Tokyo, Japan).

Transmission Electron Microscopy (TEM)

Immediately after the ophthalmectomy, the anterior segment of the rat eyes was separated and immersed in a 2.5% glutaraldehyde solution to aid in retina isolation. The retinas were then fixed with 4% glutaraldehyde for 1 hour, followed by a 2-hour rinsing period with PBS. Subsequently, the retinas were fixed with 1% osmic acid, dehydrated using ethanol, and embedded in Epon epoxy resin. The embedded samples were stained with uranium acetate and lead citrate for 15 minutes each, and ultrathin sections were cut. The retinal samples were observed and photographed using a TEM (HT7700; Exalens, Hitachi Plant Technologies Ltd, Tokyo, Japan). To measure the thickness of the basement membrane (BMT) at the intersection points with a 20-spoke grid on each capillary micrograph, at least 10 random views of the retinal capillaries extending from the outer plexiform and ganglion cell layers were selected from each rat. The thickness of the BMT of the capillaries was determined. Finally, the mean BMT value was calculated from the 4 retinas.

Terminal Deoxynucleotidyl Transferase-Mediated dUTP-Biotin Nick End Labeling (TUNEL) Staining

For the determination of DNA fragments in apoptotic cells, frozen sections of rat retina were utilized. TUNEL staining was performed following the instructions provided with the *in situ* cell death detection kit (KeyGEN BioTech Co., Ltd., Nanjing, China). In brief, the retina sections were treated with protease K at 37°C for 20 minutes, followed by incubation with the TDT enzyme solution (composed of 45

μL balanced buffer solution containing 1.0 μL biotin-11-dUTP and 4.0 μL TdT enzyme) at 37°C for 60 minutes. Subsequently, the sections were incubated with streptavidin-TRITC at 37°C for 30 minutes, rinsed with PBS and stained with 4',6-diamidino-2-phenylindole (DAPI) at room temperature for 15 minutes. The sections were observed using a confocal laser microscope (Leica, Wetzlar, Germany). The number of cells exhibiting broken DNA strands (TUNEL-positive cells) was calculated by examining 5 randomly selected fields in the retinal ganglion cell layer (GCL), inner nuclear layer (INL) and outer nuclear layer (ONL).

Flow Cytometry

Cells in the logarithmic growth phase (1×10^6) were harvested for cell cycle analysis. The cells were fixed with 70% cold ethanol and stained with 1 mL of propidium iodide (PI) dye (50 $\mu\text{g}/\text{mL}$; Becton Dickinson Biosciences, Mountain View, California USA) in a dark environment for 30 minutes. The cell cycle distribution was determined using a fluorescein isothiocyanate (FITC) FACSCalibur flow cytometer (Becton-Dickinson Biosciences, Mountain View, CA, USA). In addition, an equivalent number of cells in the logarithmic growth phase were collected for apoptosis detection. The cells were resuspended in $1 \times$ Annexin buffer and stained with 5 μL of Annexin-V-FITC (Becton-Dickinson) at room temperature for 10 minutes. Subsequently, the cells were resuspended in 300 μL of $1 \times$ Annexin buffer. The apoptosis rate was analyzed using flow cytometry.

Immunofluorescence Staining

Frozen sections of rat retina were subjected to a series of steps for immunostaining. The sections were rinsed and then permeabilized with Triton-X. To prevent nonspecific binding, a goat serum blocking solution was applied for 30 minutes. Following this, the sections were incubated overnight with a rabbit anti-rat SIRT1 polyclonal antibody (ab189494, 1:100; Abcam, Cambridge, UK). Afterward, the sections were rinsed multiple times with PBST (phosphate-buffered saline with Tween), followed by probing with the appropriate Alexa fluorescence-coupled secondary antibody (1:400) at room temperature for 3 hours. Subsequently, the sections were stained with DAPI and sealed with glycerin. Observation and imaging of the stained sections were performed with a confocal microscope. The obtained images were then analyzed using confocal software.

Reverse Transcription-Quantitative Polymerase Chain Reaction (RT-qPCR)

Total RNA content was extracted from rat retinas or hRMECs using TRIzol reagents (Invitrogen, Carlsbad, California USA) following the provided instructions. Subsequently, the extracted RNA was reverse transcribed into complementary DNA (cDNA) using the TaqMan[™] MicroRNA Assays Reverse Transcription Primer (#4427975; Applied Biosystems, Foster City, California USA). The reverse transcription reaction was carried out at 37°C for 30 minutes,

followed by a brief incubation at 85°C for 5 seconds. A 5- μL portion of the resulting cDNA was used as a template for quantitative polymerase chain reaction (qPCR) amplification, utilizing the QuantiTect SYBR Green RT-PCR kit (Applied Biosystems). The PCR reaction conditions consisted of an initial pre-denaturation step at 95°C for 5 minutes, followed by 45 cycles of denaturation at 95°C for 20 seconds, annealing at 60°C for 1 minute and extension at 72°C for 30 seconds. RT-qPCR results were analyzed using the 2-delta-delta ct (2- $\Delta\Delta\text{ct}$) method. β -actin was used as the internal reference gene. Fold changes were calculated based on relative quantification using the 2- $\Delta\Delta\text{Ct}$ method. The primer sequences used are provided in Supplementary Table 1.

Western Blot Analysis

The total protein content was extracted from rat retinas or hRMECs using the radioimmunoprecipitation assay (RIPA) lysis buffer (Sigma-Aldrich, St. Louis, Missouri USA). Following centrifugation, the protein samples were obtained from the supernatant. In the case of cultured cells, mitochondrial and cytoplasmic proteins were extracted according to the provided instructions of the mitochondrial separation kit (Thermo Fisher Scientific). The protein content was quantified using the Bradford assay. Subsequently, 40 μg of protein was separated using 10% sodium dodecyl sulfate-polyacrylamide gel electrophoresis (SDS-PAGE) and transferred onto a nitrocellulose membrane. The membrane was then blocked with 5% skimmed milk in Tris-buffered saline-Tween 20 (TBST) buffer at room temperature for 1 hour. Following blocking, the membrane was probed with specific primary antibodies against SIRT1 (ab220807, 1:1000; Abcam), β -actin (PA1-183, 1:2000; Invitrogen), inducible nitric oxide synthase (iNOS) (PA3-030A; 1:2000, Invitrogen), Cytochrome c (Cyt c; ab90529, 1:1000; Abcam), cytochrome oxidase (COX) IV (Bioworld Technology, St. Louis, Minnesota USA), cleaved caspase-3 (ab13847, 1:500; Abcam), glyceraldehyde-3-phosphate dehydrogenase (GAPDH; ab9485, 1:2500; Abcam), and vascular endothelial growth factor (VEGF) (#PA5-16754, 1:1000; Thermo Fisher Scientific) at 4°C overnight. Afterward, the membranes were incubated with a horseradish peroxidase (HRP)-conjugated secondary antibody, specifically goat anti-rabbit IgG (#656120, 1:4000; Invitrogen), at room temperature for 1 hour. β -actin was used as an internal reference.

The immunocomplexes on the membrane were visualized using an enhanced chemiluminescence reagent (ECL) (Amersham Pharmacia Biotech, Piscataway, New Jersey USA), and the band intensities were quantified using Image-Pro Plus 9.0 software (Media Cybernetics, Inc., Rockville, Maryland USA).

Statistical Analysis

All statistical analyses were conducted using IBM[™] SPSS 21.0 statistical software (IBM Corp., Armonk, New York USA). The measurement data were presented as mean \pm standard deviation (SD). The comparison between multiple

groups was performed using one-way analysis of variance (ANOVA) followed by Tukey's post hoc test. Statistical significance was considered when $P < .05$.

RESULTS

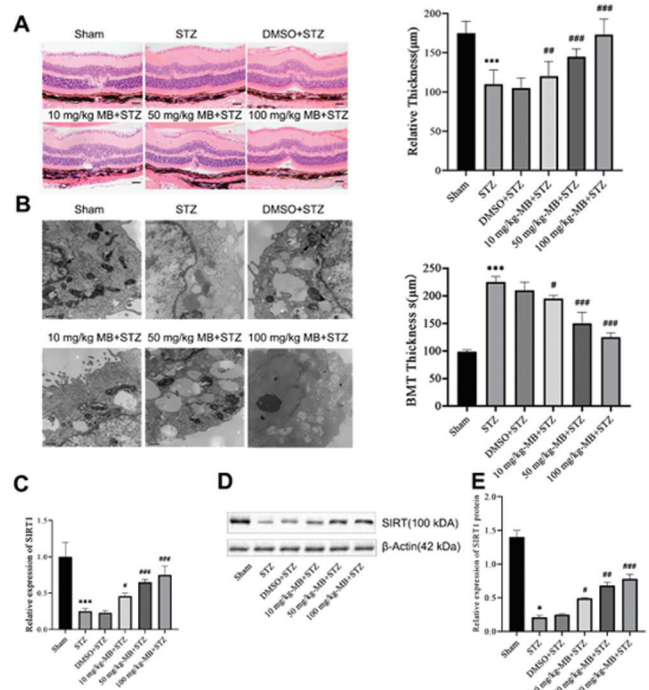
MB Treatment Effectively Rescues the Low Expression of SIRT1 Observed in the STZ-Induced Rat DR Model

In this study, a rat model of DR was established by administering a dose of 60 mg/kg STZ via intraperitoneal injection. Successful model establishment was confirmed by a blood glucose level >16.7 mmol/L at 48 hours. Age-matched sham-operated rats received an equivalent volume of sodium citrate prior to treatment with MB. A total of 2 weeks after STZ induction, the rats were treated with different doses of MB (DMSO, 10 mg/kg MB, 50 mg/kg MB and 100 mg/kg MB). H&E staining was performed to assess the structural integrity of retinal tissues in the DR-induced rats. The results showed that compared with the sham-operated rats, the STZ-treated rats exhibited signs of edema, capillary wall thickening, endothelial cell hyperplasia and fibrous tissue hyperplasia. However, these pathological changes were partially alleviated in a dose-dependent manner by MB treatment (Figure 1A). Furthermore, TEM was used to examine the ultrastructure of the retinas. The BMT in the STZ-treated rats was increased compared with the sham-operated rats. However, treatment with MB led to a dose-dependent decrease in BMT values (Figure 1B). The expression levels of SIRT1 were assessed using RT-qPCR and Western blot analysis. The results revealed that the expression of SIRT1 was significantly reduced in the retinas of STZ-treated rats compared with the sham-operated rats. However, MB treatment effectively restored the expression of SIRT1 in a dose-dependent manner (Figure 1C, 1D). These findings suggest that the expression of SIRT1 is suppressed in STZ-induced rats, and MB treatment can increase the expression of SIRT1 in this DR model.

MB Treatment Demonstrated Significant Alleviation of Oxidative Stress, Inflammation and Apoptosis in the Retinas of Rats with DR

The expression patterns of oxidative stress-related factors in the retinal tissues of STZ-treated rats were examined using dichlorodihydrofluorescein (DCFDA) and lipid peroxidation MDA assay kits. The results demonstrated a significant increase in ROS and MDA levels, along with a decrease in SOD level, in the retinal tissues of STZ-injected rats compared with the sham-operated rats. However, treatment with MB in a dose-dependent manner effectively reversed these changes, indicating a reduction in oxidative stress (Figure 2; Table 1). Furthermore, RT-qPCR and Western blot analysis revealed that the expression of iNOS was notably elevated in the retinal tissues of STZ-treated rats compared with the sham-operated rats. However, treatment with MB inhibited the STZ-induced upregulation of iNOS expression in a dose-dependent manner (Figure 3A, 3B). Nitrite testing demonstrated that the elevated levels of NO observed in STZ-treated rats were dose-

Figure 1. Downregulation of SIRT1 in STZ-induced Rat with DR model. Rats treated with STZ were further subjected to DMSO, 10 mg/kg MB, 50 mg/kg MB, and 100 mg/kg MB treatment, with each treatment group containing 15 rats. (1A) Representative micrographs of retinal tissues using H&E staining (at 400x magnification) (scale bar = 25 μ m) and accompanying thickness quantification analysis. * $P < .05$ when compared with sham-operated rats, and # $P < .05$ relative to STZ-treated rats. (1B) Retinal tissue ultrastructure of rats observed under a TEM (at 10000x magnification) (scale bar = 1 μ m). The arrow signifies the capillary BMT, which is measured for membrane width. (1C) SIRT1 expression patterns in rat retinal tissues, measured via RT-qPCR, normalized to β -actin. (1D) Illustrative Western blots of SIRT1 protein and its quantification in rat retinal tissues, normalized to β -actin. * $P < .05$, ** $P < .01$, *** $P < .001$ denote comparisons with sham-operated rats; # $P < .05$, ## $P < .01$, ### $P < .001$ signifies comparisons with STZ-injected rats treated with DMSO. The results are expressed as mean \pm standard deviation and were analyzed by one-way ANOVA with Tukey's post hoc test; n = 15.

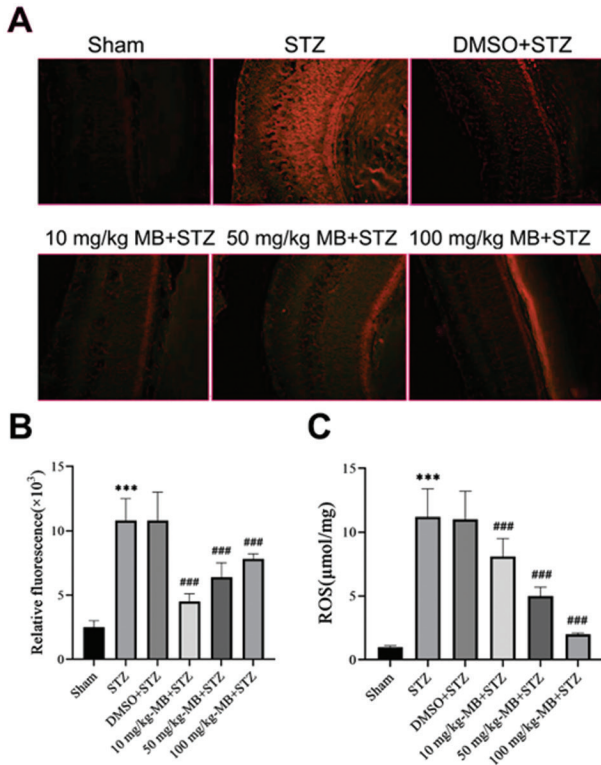


Abbreviations: ANOVA, analysis of variance; BMT, basement membrane; DM, diabetes mellitus; DMSO, dimethyl sulfoxide; DR, diabetic retinopathy; GCL, ganglion cell layer; H&E, hematoxylin-eosin; IPL, inner plexiform layer; ONL, outer nuclear layer; OPL, outer plexiform layer; RT-qPCR, reverse transcription-quantitative polymerase chain reaction; SIRT1, Sirtuin 1; STZ, streptozotocin; TEM, transmission electron microscopy.

dependently decreased upon MB treatment (Figure 3C). In addition, ELISA results showed a significant increase in the contents of IL-6, TNF- α and CRP in the cell supernatant of STZ-treated rats compared with the sham-operated rats.

In contrast, MB treatment effectively reduced the expression levels of IL-6, TNF- α and CRP in a dose-dependent manner, indicating its anti-inflammatory effect (Figure 3D-3F). TUNEL staining revealed an increase in cell apoptosis in STZ-treated rats, whereas subsequent treatment with MB resulted in dose-dependent reductions in cell apoptosis (Figure 3G, 3H). Western blot analysis showed that the protein expression of cleaved caspase-3, an apoptosis-related factor, was higher in the retinal tissues of the STZ-treated rats compared with the sham-operated rats.

Figure 2. MB reduces ROS level in retinal tissues of rats with DR. (2A) Representative images displaying ROS via CM-H2DCFDA staining (red) in retinal tissues from sham-operated and STZ-treated rats treated with DMSO, 10 mg/kg MB, 50 mg/kg MB and 100 mg/kg MB (at 400x magnification) (scale bar = 25 μ m). (2B) Relative fluorescence intensity in retinal tissues. (2C) Quantitative analysis of ROS content in retinal tissues. **P* < .05, ***P* < .01, ****P* < .001 denote comparisons with sham-operated rats; #*P* < .05, ##*P* < .01, ###*P* < .001 represent comparisons with STZ-injected rats treated with DMSO. Data are expressed as mean \pm standard deviation. Comparisons between multiple groups were analyzed by one-way ANOVA with Tukey's post hoc test, n = 5.



Abbreviations: ANOVA, analysis of variance; DMSO, dimethyl sulfoxide; DR, diabetic retinopathy; MB, methylene blue; ROS, reactive oxygen species; STZ, streptozotocin.

Table 1. Methylene Blue Reduced the Expression of 3,4-methylenedioxyamphetamine While Increasing That of Superoxide Dismutase in Retinal Tissues of Streptozotocin-Treated Rats

Group	SOD (U/mg)	MDA (μ mol/mg)
Sham	22.97 \pm 1.78	2.63 \pm 0.29
STZ	8.48 \pm 0.97 ^a	7.33 \pm 0.65 ^a
STZ + DMSO	8.59 \pm 0.93	7.21 \pm 0.69
10 mg/kg-MB + STZ	12.39 \pm 1.27 ^b	6.35 \pm 0.75 ^b
50 mg/kg-MB + STZ	17.39 \pm 1.75 ^b	5.12 \pm 0.39 ^b

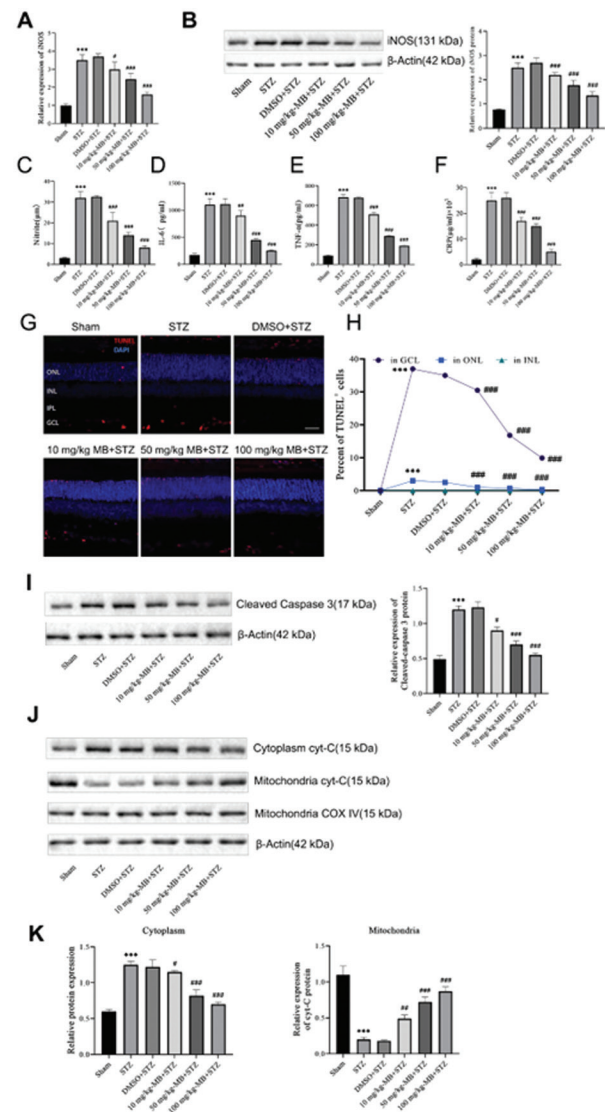
^a*P* < .05 compared with the sham-operated rats

^b*P* < .05 compared with the rats injected with STZ + DMSO

Notes: MDA level was detected using lipid peroxidation MDA assay and SOD was detected by CCK-8 SOD assay. Data were shown as mean \pm standard deviation and compared using one-way ANOVA with Tukey's post hoc test. n=15 for rats at each treatment.

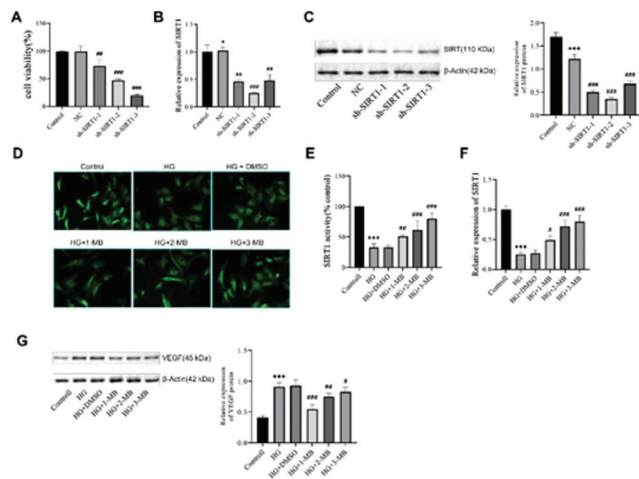
Abbreviations: ANOVA, one-way analysis of variance; CCK-8, Cell Counting Kit-8; DMSO, dimethyl sulfoxide; MB, methylene blue; MDA, 3,4-methylenedioxyamphetamine; SOD, superoxide dismutase; STZ, streptozotocin.

Figure 3. MB mitigates oxidative stress, inflammation and apoptosis in rats with DR. STZ-administered rats were exposed to DMSO, 10 mg/kg MB, 50 mg/kg MB and 100 mg/kg MB; each treatment group comprised 15 rats. (3A) iNOS expression profile measured via RT-qPCR in rat retinal tissues, normalized to β -actin. (3B) Representative Western blots of iNOS protein and their respective quantitation in rat retinal tissues, normalized to β -actin. (3C) NO expression assessed via nitrite test in rat retinal tissues. (3D-3F) IL-6 (3D), TNF- α (3E) and CRP (3F) expression profiles measured by ELISA in the cell supernatant. (3G, 3H) Representative images of apoptotic cells (at 400x magnification) (scale bar = 25 μ m) (3G) and cell apoptosis quantitation in rat retinal tissues (3H) via TUNEL staining. (3I) Representative Western blots of cleaved caspase-3 protein and their quantitation in rat retinal tissues, normalized to β -actin. (3J, 3K) Representative Western blots of cyt-c protein and its quantitation in the cytoplasm and mitochondria, normalized to β -actin. Symbols **P* < .05, ***P* < .01, ****P* < .001 denote comparisons to sham-operated rats, while #*P* < .05, ##*P* < .01, ###*P* < .001 signify comparisons to STZ-injected rats treated with DMSO. The data are expressed as mean \pm standard deviation, and multiple group comparisons were analyzed by one-way ANOVA with Tukey's post hoc test (n = 15).



Abbreviations: ANOVA, analysis of variance; CRP, C-reactive protein; Cyt c, Cytochrome c; DMSO, dimethyl sulfoxide; DR, diabetic retinopathy; ELISA, enzyme-linked immunosorbent assay; GCL, ganglion cell layer; IL-6, interleukin-6; INL, inner nuclear layer; iNOS, inducible nitric oxide synthase; MB, methylene blue; NO, nitric oxide; ONL, outer nuclear layer; RT-qPCR, reverse transcription-quantitative polymerase chain reaction; STZ, streptozotocin; TNF- α , tumor necrosis factor α ; TUNEL, Terminal Deoxynucleotidyl Transferase-Mediated dUTP-Biotin Nick End Labeling

Figure 4. MB activates SIRT1 expression in high glucose-treated hRMECs. hRMECs were transfected with sh-SIRT1-1, sh-SIRT1-2 or sh-SIRT1-3, and high glucose-exposed hRMECs were administered DMSO, 1-MB, 2-MB or 3-MB, respectively. (4A) Cell viability was assessed via CCK-8 assay. (4B) SIRT1 expression profile determined by RT-qPCR in hRMECs, normalized to β -actin. (4C) Representative Western blots of SIRT1 protein and their quantitation in hRMECs, normalized to β -actin. (4D, 4E) Representative images (at 400x magnification) (scale bar = 25 μ m) (4D) and SIRT1 activity and nuclear accumulation in hRMECs (4E) as detected by immunofluorescence staining. (4F) SIRT1 expression profile assessed by RT-qPCR in hRMECs, normalized to β -actin. (4G) Representative Western blots of VEGF protein and its quantitation in hRMECs, normalized to β -actin. Comparisons were made with control cells ($*P < .05$, $**P < .01$, $***P < .001$) and with cells stimulated with NC or HG + DMSO ($\#P < .05$, $\#\#P < .01$, $\#\#\#P < .001$). Results are expressed as mean \pm standard deviation. Multiple group comparisons were analyzed by one-way ANOVA with Tukey's post hoc test. Cell experiments were conducted 3 times independently.

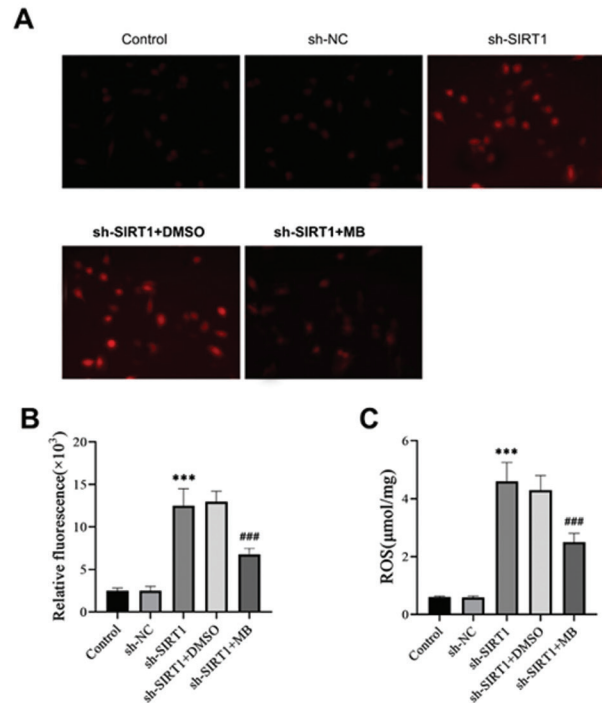


Abbreviations: ANOVA, analysis of variance; CCK-8, Cell Counting Kit-8; DMSO, dimethyl sulfoxide; HG, high glucose; hRMECs, human retinal microvascular endothelial cells; MB, methylene blue; NC, negative control; RT-qPCR, reverse transcription-quantitative polymerase chain reaction; SIRT1, sirtuin 1; VEGF, vascular endothelial growth factors.

However, MB treatment dose-dependently reduced the expression of cleaved caspase-3 (Figure 3I). Furthermore, changes in the expression of cytoplasmic and mitochondrial Cyt c were observed. The cytoplasmic expression of Cyt c was elevated in the retinal tissues of STZ-treated rats, which was decreased by MB treatment. Conversely, MB treatment led to increased expression of Cyt c in the mitochondria (Figure 3J, 3K). MB treatment resulted in the activation of SIRT1 expression in hRMECs exposed to HG conditions.

After confirming the ability of MB to increase SIRT1 expression in STZ-treated rats, our focus shifted to examining the interaction between MB and SIRT1 in hRMECs exposed to HG conditions. To investigate this, we conducted SIRT1 loss-of-function and rescue experiments in hRMECs. We first assessed cell viability following transfection with sh-SIRT1-1, sh-SIRT1-2 or sh-SIRT1-3. The results showed a decrease in cell viability at 48 hours post-transfection (Figure 4A). RT-qPCR and Western blot analysis confirmed reduced SIRT1 expression in hRMECs transfected with sh-SIRT1-1, sh-SIRT1-2 or sh-SIRT1-3, with sh-SIRT1-2 demonstrating the strongest silencing effect and thus selected for subsequent experiments (Figure 4B, 4C). Immunofluorescence staining

Figure 5. MB reduces ROS level in HG-treated hRMECs. (5A) Representative images of ROS, depicted by CM-H2DCFDA staining (green), in hRMECs treated with sh-NC, sh-SIRT1, sh-SIRT1 + DMSO and sh-SIRT1 + MB, respectively (at 400x magnification) (scale bar = 25 μ m). (5B) Relative fluorescence in hRMECs. (5C) Quantitative analysis of ROS content in hRMECs. $*P < .05$, $**P < .01$, $***P < .001$ represent comparisons with sh-NC-treated hRMECs, while $\#P < .05$, $\#\#P < .01$, $\#\#\#P < .001$ denote comparisons with hRMECs treated with sh-SIRT1 + DMSO. The data are expressed as mean \pm standard deviation, and comparisons between multiple groups were analyzed by one-way ANOVA with Tukey's post hoc test. The cell experiments were performed 3 times independently.



Abbreviations: ANOVA, analysis of variance; CCK-8, Cell Counting Kit-8; DMSO, dimethyl sulfoxide; HG, high glucose; hRMECs, human retinal microvascular endothelial cells; MB, methylene blue; NC, negative control; ROS, reactive oxygen species; RT-qPCR, reverse transcription-quantitative polymerase chain reaction; SIRT1, sirtuin 1.

Table 2. Methylene Blue Reduced the Expression of 3,4-methylenedioxyamphetamine While Increasing That of Superoxide Dismutase in Human Retinal Microvascular Endothelial Cells hRMECs by Upregulating Sirtuin 1

Group	SOD (U/mg)	MDA (umol/mg)
Control	25.29 \pm 3.97	2.77 \pm 0.29
sh-NC	26.35 \pm 2.41	2.12 \pm 0.23
sh-SIRT1	7.88 \pm 0.59 ^a	15.16 \pm 1.27 ^a
sh-SIRT1 + DMSO	7.64 \pm 0.39	15.29 \pm 1.37
sh-SIRT1 + MB	17.43 \pm 1.85 ^b	8.91 \pm 0.69 ^b

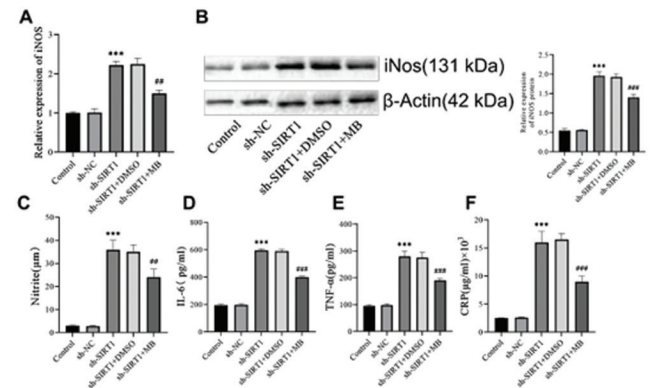
^a $P < .05$ compared with cells treated with sh-NC

^b $P < .05$ compared with cells treated with sh-SIRT1 + DMSO

Notes: MDA level was detected using lipid peroxidation MDA assay and SOD was detected by CCK-8 SOD assay. Data were shown as mean \pm standard deviation and compared using one-way ANOVA with Tukey's post hoc test. The cell experiment was repeated independently 3 times.

Abbreviations: CCK-8, Cell Counting Kit-8; DMSO, dimethyl sulfoxide; hRMECs, human retinal microvascular endothelial cells; MB, methylene blue; MDA, 3,4-methylenedioxyamphetamine; sh-NC, short hairpin RNA-negative control; SIRT1, sirtuin 1; SOD, superoxide dismutase

Figure 6. MB mitigates HG-induced oxidative stress and inflammation in hRMECs via SIRT1 activation. hRMECs were treated with sh-NC, sh-SIRT1, sh-SIRT1 + DMSO, and sh-SIRT1 + MB, respectively. (6A) iNOS expression profile assessed by RT-qPCR in hRMECs, normalized to β -actin. (6B) Representative Western blots of iNOS protein and their respective quantitation in hRMECs, normalized to β -actin. (6C) NO expression profile measured by nitrite test in hRMECs. (6D-6F) IL-6 (6D), TNF- α (6E), and CRP (6F) expression profiles determined by ELISA in the cell supernatant. * $P < .05$, ** $P < .01$, *** $P < .001$ indicate comparisons with sh-NC-treated cells, and # $P < .05$, ## $P < .01$, ### $P < .001$ represent comparisons with cells treated with sh-SIRT1 + DMSO. The data are presented as mean \pm standard deviation. Multiple group comparisons were analyzed by one-way ANOVA with Tukey's post hoc test. Cell experiments were performed 3 times independently.



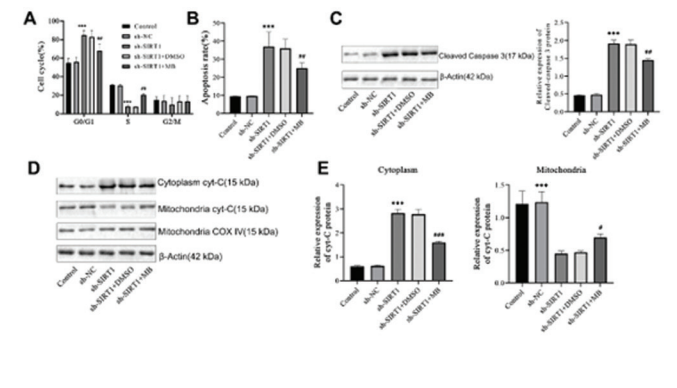
Abbreviations: ANOVA, analysis of variance; CRP, C-reactive protein; DMSO, dimethyl sulfoxide; ELISA, enzyme-linked immunosorbent assay; HG, high glucose; hRMECs, human retinal microvascular endothelial cells; IL-6, interleukin-6; iNOS, inducible nitric oxide synthase; MB, methylene blue; NC, negative control; NO, nitric oxide; RT-qPCR, reverse transcription-quantitative polymerase chain reaction; sh-SIRT1, short hairpin RNA; SIRT1, sirtuin 1; TNF- α , tumor necrosis factor α .

revealed that HG stimulation led to reduced SIRT1 activity and nuclear accumulation in hRMECs. However, treatment with MB resulted in dose-dependent increases in SIRT1 levels in HG-exposed hRMECs, with 3-MB showing the most pronounced elevation (Figure 4D, 4E). RT-qPCR analysis further confirmed that SIRT1 expression was decreased in hRMECs stimulated with HG, while MB treatment dose-dependently increased SIRT1 expression, with 3-MB yielding the highest levels (Figure 4F). In addition, we assessed the effect of MB on vascular endothelial growth factor (VEGF) protein expression using Western blot analysis. The results demonstrated an increase in VEGF protein levels in HG-treated hRMECs, which were subsequently decreased in a dose-dependent manner with further MB treatment (Figure 4G).

In hRMECs, MB Treatment Effectively Suppressed Oxidative Stress and Inflammation Through the Activation of SIRT1

To investigate the role of SIRT1 in mediating the effects of MB on oxidative stress and inflammation, we conducted experiments to silence SIRT1 expression in hRMECs. Silencing of SIRT1 in hRMECs resulted in increased levels of ROS and lipid peroxidation marker MDA, as well as decreased SOD activity, indicating enhanced oxidative stress. However, treatment with MB reversed these effects of SIRT1 silencing on oxidative stress-related factors in hRMECs (Figure 5, Table 2). Moreover, the expression of iNOS was upregulated

Figure 7. MB suppressed the apoptosis of HG-treated hRMECs. hRMECs were treated with sh-NC, sh-SIRT1, sh-SIRT1 + DMSO and sh-SIRT1 + MB, respectively. (7A) Cell cycle distribution as determined by flow cytometry analysis. (7B) Cell apoptosis as determined by flow cytometry analysis. (7C) Representative Western blots of cleaved caspase-3 protein and its quantitation in hRMECs, normalized to β -actin. (7D, 7E) Western blots of Cytochrome c protein (7D) and its quantitation (7E) in the cytoplasm and mitochondria, normalized to β -actin. * $P < .05$, ** $P < .01$, *** $P < .001$, compared with sh-NC-treated cells, and # $P < .05$, ## $P < .01$, ### $P < .001$, compared with cells stimulated with sh-SIRT1 + DMSO. The results were the measurement data and expressed as mean \pm standard deviation. Comparisons between multiple groups were analyzed by one-way ANOVA with Tukey's post hoc test. The cell experiments were repeated 3 times independently.



Abbreviations: ANOVA, analysis of variance; Cyt c, cytochrome c; DMSO, dimethyl sulfoxide; HG, high glucose; hRMECs, human retinal microvascular endothelial cells; MB, methylene blue; NC, negative control; NO, nitric oxide; sh-NC, short hairpin RNA-negative control; SIRT1, sirtuin 1.

in hRMECs upon SIRT1 silencing, but this increase was attenuated by MB treatment (Figure 6A, 6B). The levels of NO, as measured by the nitrite test, were elevated in SIRT1-silenced hRMECs, but MB treatment effectively reversed this effect (Figure 6C). Furthermore, the concentrations of inflammatory markers IL-6, TNF- α and CRP increased in hRMECs following SIRT1 knockdown. However, co-treatment with MB reversed these elevations, indicating the anti-inflammatory effects of MB (Figure 6D-6F).

MB Mitigates Apoptosis in hRMECs Exposed to High Glucose Conditions

Finally, we investigated the involvement of SIRT1 in the anti-apoptotic effects of MB in hRMECs. To evaluate cell apoptosis and the expression of apoptosis-related factors, we performed experiments involving SIRT1 knockdown and MB treatment in hRMECs. FC analysis revealed that SIRT1 knockdown increased the apoptosis rate of hRMECs, while MB treatment reversed this effect (Figure 7A, 7B). In addition, Western blot analysis demonstrated that hRMECs treated with sh-SIRT1 exhibited higher levels of cleaved caspase-3, which were reduced by MB treatment (Figure 7C). Moreover, the expression of Cyt c protein in the cytoplasm of hRMECs was enhanced upon SIRT1 knockdown, but this elevation was suppressed by MB treatment (Figure 7D, 7E). Collectively, these findings indicate that MB inhibits apoptosis in hRMECs by activating SIRT1 expression.

DISCUSSION

DR is a progressive ophthalmic condition that occurs due to long-term exposure to chronic hyperglycemia in patients with diabetes, resulting in pathological changes in the retina. Various treatment approaches, including physical exercise and drug therapy, have been shown to be effective in slowing down the progression of DR.²⁷ Previous research has suggested that phytoestrogens like biochanin A may have therapeutic potential in DR.²⁸ In our study, we aimed to investigate the role of MB and SIRT1 in oxidative stress, inflammation and cell apoptosis using a rat model of STZ-induced DR.

Our initial findings revealed that SIRT1 expression was reduced in the retinal tissues of rats with STZ-induced DR. SIRT1 is a nuclear protein involved in regulating inflammation, apoptosis and other metabolic pathways through histone and non-histone deacetylation.²⁹ Consistent with our findings, other studies have also reported downregulation of SIRT1 in endothelial cells of mice with diabetes,³⁰ while activation of retinal SIRT1 has shown protective effects against retinal damage in diabetes.³

Next, we explored the relationship between MB and SIRT1 in rats with DR and found that MB treatment could stimulate SIRT1 expression, indicating an association between the effects of MB on DR and SIRT1. Furthermore, our results demonstrated that MB inhibited oxidative stress and inflammatory response in rats with DR by activating SIRT1. This was evident from the decreased levels of ROS, MDA, iNOS, NO and inflammatory factors, as well as the increased activity of SOD. Oxidative stress and inflammation are key contributors to the progression of DR, and previous studies have shown that MB can reduce oxidative stress and inhibit inflammation.³² The activation of SIRT1 has also been associated with decreased oxidative stress and inflammation in DR.³³

In addition, our findings showed that MB suppressed apoptosis in hRMECs, thus ameliorating DR through the activation of SIRT1. This was supported by the decreased levels of Cyt c and caspase-3, which are markers of apoptosis.³⁴ Previous research has highlighted the anti-apoptotic effects of phytoestrogens, including MB, and their ability to interact with estrogen.³⁵ Activation of SIRT1 has also been shown to suppress apoptosis in retinal cells and inhibit apoptosis and inflammation in DR.³⁶

CONCLUSION

Our study provides evidence that MB can inhibit oxidative stress, inflammation, and cell apoptosis in rats with DR by activating SIRT1. These findings have potential therapeutic implications for the treatment of oxidative stress and inflammatory response in patients with DR. Further research and clinical studies are warranted to explore the therapeutic benefits of MB in the management of DR.

ACKNOWLEDGMENTS

We extend our sincere gratitude to our colleagues for their invaluable contributions and insightful feedback on this manuscript.

CONFLICT OF INTEREST

None.

REFERENCES

- Kropp M, Golubnitschaja O, Mazurakova A, et al. Diabetic retinopathy as the leading cause of blindness and early predictor of cascading complications-risks and mitigation. *EPMA J*. 2023;14(1):21-42. doi:10.1007/s13167-023-00314-8
- Sasongko MB, Wardhana FS, Febranto GA, et al. The estimated healthcare cost of diabetic retinopathy in Indonesia and its projection for 2025. *Br J Ophthalmol*. 2020;104(4):487-492. doi:10.1136/bjophthalmol-2019-313997
- Debele GR, Kanfe SG, Weldesenbet AB, Ayana GM, Jifar WW, Ruru TB. Incidence of diabetic retinopathy and its predictors among newly diagnosed type 1 and type 2 diabetic patients: a retrospective follow-up study at tertiary health-care setting of Ethiopia J. *Diabetes Metab Syndr Obes*. 2021;14:1305-1313. doi:10.2147/DMSO.S300373
- Ansari P, Tabasumma N, Snigdha NN, et al. Diabetic retinopathy: an overview on mechanisms, pathophysiology and pharmacotherapy J. *Diabetology*. 2022;3(1):159-175. doi:10.3390/diabetology3010011
- Yang L, Youngblood H, Wu C, Zhang Q. Mitochondria as a target for neuroprotection: role of methylene blue and photobiomodulation. *Transl Neurodegener*. 2020;9(1):19. doi:10.1186/s40035-020-00197-z
- Frank RN. Diabetic retinopathy and systemic factors. *Middle East Afr J Ophthalmol*. 2015;22(2):151-156. doi:10.4103/0974-9233.154388
- Bhattacharjee H, Barman M, Garg M. *Diabetic Retinopathy and Diabetic Macular Edema: Fighting the Emerging Global Burden M. Diabetic Macular Edema*. Springer; 2023:221-227.
- PA Senior, Houlden RL, KIM J, et al. Pharmacologic glycemic management of type 2 diabetes in adults: 2020 update—the user's guide J. *Canadian journal of diabetes*, 2020, 44(7): 592-6.
- Sun J, Nie H, Pan P, et al. Combined Anti-Angiogenic and Anti-Inflammatory Nanoformulation for Effective Treatment of Ocular Vascular Diseases. *Int J Nanomedicine*. 2023;18:437-453. doi:10.2147/IJN.S387428
- Simó R, Hernández C. New Insights into Treating Early and Advanced Stage Diabetic Retinopathy. *Int J Mol Sci*. 2022;23(15):8513. doi:10.3390/ijms23158513
- Zaino B, Goel R, Devaragudi S, et al. Diabetic neuropathy: pathogenesis and evolving principles of management. *Dis Mon*. 2023;101582. doi:10.1016/j.disamonth.2023.101582
- Chan TC, Wilkinson Berka JL, Deliyanti D, et al. The role of reactive oxygen species in the pathogenesis and treatment of retinal diseases. *Exp Eye Res*. 2020;201:108255. doi:10.1016/j.exer.2020.108255
- Thatcher TH. *PETERS-GOLDEN M. From Biomarker to Mechanism? F2-isoprostanes in Pulmonary Fibrosis Z. American Thoracic Society*; 2022:530-532.
- Bokhary K, Aljaser F, Abudawood M, et al. Role of oxidative stress and severity of diabetic retinopathy in type 1 and type 2 diabetes J. *Ophthalmic Res*. 2021;64(4):613-621. doi:10.1159/000514722
- Naughton SX, Beck WD, Wei Z, Wu G, Terry AV Jr. Multifunctional compounds lithium chloride and methylene blue attenuate the negative effects of diisopropylfluorophosphate on axonal transport in rat cortical neurons. *Toxicology*. 2020;431:152379. doi:10.1016/j.tox.2020.152379
- Khan I, Saeed K, Zekker I, et al. Review on methylene blue: its properties, uses, toxicity and photodegradation J. *Water*. 2022;14(2):242. doi:10.3390/w14020242
- Din MI, Khalid R, Najeeb J, Hussain Z. Fundamentals and photocatalysis of methylene blue dye using various nanocatalytic assemblies—a critical review J. *J Clean Prod*. 2021;298:126567. doi:10.1016/j.jclepro.2021.126567
- Nedu M-E, Tertis M, Cristea C, Georgescu AV. Comparative study regarding the properties of methylene blue and proflavine and their optimal concentrations for in vitro and in vivo applications J. *Diagnostics (Basel)*. 2020;10(4):223. doi:10.3390/diagnostics10040223
- Hamper M, Cassano P, Lombard J. Treatment of Kleine-Levin syndrome with intranasal photobiomodulation and methylene blue J. *Cureus*. 2021;13(10):e18596. doi:10.7759/cureus.18596
- Chen D, Wang Y-Y, Li S-P, et al. Maternal propionate supplementation ameliorates glucose and lipid metabolic disturbance in hypoxia-induced fetal growth restriction. *Food Funct*. 2022;13(20):10724-10736. doi:10.1039/D2FO01481E
- Alda M. Methylene blue in the treatment of neuropsychiatric disorders J. *CNS Drugs*. 2019;33(8):719-725. doi:10.1007/s40263-019-00641-3
- Sulek A, Pucelik B, Kobielski Z, Barzowska A, Dąbrowski JM. Photodynamic inactivation of bacteria with porphyrin derivatives: effect of charge, lipophilicity, ROS generation, and cellular uptake on their biological activity in vitro J. *Int J Mol Sci*. 2020;21(22):8716. doi:10.3390/ijms21228716
- Shin SY, Kim TH, Wu H, Choi YH, Kim SG. SIRT1 activation by methylene blue, a repurposed drug, leads to AMPK-mediated inhibition of steatosis and steatohepatitis. *Eur J Pharmacol*. 2014;727:115-124. doi:10.1016/j.ejphar.2014.01.035
- Maghbooli Z, Emamgholipour S, Aliakbar S, Amini M, Gorgani-Firuzjaee S, Hossein-Nezhad A. Differential expressions of SIRT1, SIRT3, and SIRT4 in peripheral blood mononuclear cells from patients with type 2 diabetic retinopathy. *Arch Physiol Biochem*. 2020;126(4):363-368. doi:10.1080/13813455.2018.1543328
- Oza MJ, Kulkarni YA. Biochanin A improves insulin sensitivity and controls hyperglycemia in type 2 diabetes. *Biomed Pharmacother*. 2018;107:1119-1127. doi:10.1016/j.biopha.2018.08.073
- Liu Y, Zheng Y, Zhou Y, et al. The expression and significance of mTORC1 in diabetic retinopathy J. *BMC Ophthalmol*. 2020;20(1):1-7. doi:10.1186/s12886-020-01553-3
- Amato R, Catalani E, Dal Monte M, et al. Morpho-functional analysis of the early changes induced in retinal ganglion cells by the onset of diabetic retinopathy: The effects of a neuroprotective strategy J. 2022, 185: 106516.
- Felix F B, Vago J P, Beltrami V A, et al. Biochanin A as a modulator of the inflammatory response: An updated overview and therapeutic potential J. 2022: 106246.
- De Gregorio E, Colell A, Morales A, et al. Relevance of SIRT1-NF-κB axis as therapeutic target to ameliorate inflammation in liver disease J. 2020, 21(11): 3858. doi:10.3390/ijms21113858
- Li X, Wu G, Han F, et al. SIRT1 activation promotes angiogenesis in diabetic wounds by protecting endothelial cells against oxidative stress J. 2019, 661: 117-24.
- Tu Y, Song E, Wang Z, et al. Melatonin attenuates oxidative stress and inflammation of Müller cells in diabetic retinopathy via activating the Sirt1 pathway J. 2021, 137: 111274. doi:10.1016/j.biopha.2021.111274
- Wang M-H, Hsiao G, AL-SHABRAWAY M J A. Eicosanoids and oxidative stress in diabetic retinopathy J. 2020, 9(6): 520.
- Kim H, Baek [C]M. High-Grade Endometrioid Stromal Sarcoma of the Ovary: Malignant Transformation of Ovarian Mature Cystic Teratoma. *Medicina (Kaunas)*. 2022;58(10):1501. doi:10.3390/medicina58101501

34. Li X, Fang F, Gao Y, et al. ROS induced by KillerRed targeting mitochondria (mtKR) enhances apoptosis caused by radiation via Cyt c/caspase-3 pathway J. 2019, 2019.
35. Huang S, Qi B, Yang L, et al. Phytoestrogens, novel dietary supplements for breast cancer J. 2023, 160: 114341. doi:10.1016/j.biopha.2023.114341
36. Kang Q, Yang C J R B. Oxidative stress and diabetic retinopathy: Molecular mechanisms, pathogenetic role and therapeutic implications J. 2020, 37: 101799.

Supplementary Table 1. Primer sequences for RT-qPCR

Gene	Primer sequence
Rat β -actin	F: 5'-TCCTCCTGAGCGCAAGTACTCT-3' R: 5'-GCTCAGTAACAGTCCGCCTAGAA-3'
Rat SIRT1	F: 5'-CGCCTTATCCTCTAGTTCCTGTG-3' R: 5'-CGGTCTGTCAGCATCATCTTCC-3'
Rat iNOS	F: 5'-ATTCAGATCCCGAAACGC-3' R: 5'-CCAGAACCTCCAGGCACA-3'
Human β -actin	F: 5'-TGCTCGACAACGGCTCCGGCATGT-3' R: 5'-CCAGCCAGGTCCAGACGCAGGAT-3'
Human SIRT1	F: 5'-GAAAATGCTGGCCTAATAGACTTG-3' R: 5'-TGGTACAAACAAGTATTGATTACCG-3'
Human iNOS	F: 5'-TCACGACACCCTCACCACAA-3' R: 5'-CCATCCTCCTGCCCACTTCCTC-3'

Abbreviations: RT-qPCR, reverse transcription-quantitative polymerase chain reaction; SIRT1, sirtuin 1; iNOS, inducible nitric oxide synthase; F, forward; R, reverse.